



## Effect of Dy addition on microstructure and mechanical properties of Mg–4Y–3Nd–0.4Zr alloy

Hong-hui LIU<sup>1,2</sup>, Zhi-liang NING<sup>1,2</sup>, Jun-ying YI<sup>1,3</sup>, Qian MA<sup>4</sup>,  
Hai-chao SUN<sup>1,2</sup>, Yong-jiang HUANG<sup>1,2</sup>, Jian-fei SUN<sup>1,2</sup>

1. School of Materials Science and Engineering, Harbin Institute of Technology, Harbin 150001, China;
2. National Key laboratory for Precision Hot Processing of Metals, Harbin Institute of Technology, Harbin 150001, China;
3. School of Materials Science and Engineering, Jiangsu University of Science and Technology, Zhangjiagang 215600, China;
4. Mechanical and Manufacturing Engineering and Design Research Institute, School of Aerospace, RMIT University, GPO Box 2476, Melbourne, VIC 3001, Australia

Received 25 January 2016; accepted 26 August 2016

**Abstract:** Minor Dy element was added into a Mg–4Y–3Nd–0.4Zr alloy, and its effects on the microstructure and the mechanical properties at elevated temperatures were investigated. Scanning electron microscope (SEM) and transmission electron microscope (TEM) were used to observe the microstructures. The results indicated that the as-cast eutectic and isolated cuboid-shaped Mg–RE phases were Mg<sub>5</sub>RE and Mg<sub>3</sub>RE<sub>17</sub>, respectively, and distributed mainly along grain boundaries. After a solution treatment, the eutectic Mg<sub>5</sub>RE phases were dissolved into the matrix, whereas the Mg<sub>3</sub>RE<sub>17</sub> compound still remained. After peak aging, fine Mg–RE phases were precipitated homogeneously within the matrix of the alloys containing Dy. Dy addition can result in a significant improvement in the tensile strength at both room and elevated temperatures, and a slight decrease in the elongation.

**Key words:** magnesium alloy; Dy addition; microstructure; mechanical property

### 1 Introduction

Magnesium alloys have found applications in many industries due to their light mass and other attractive characteristics [1,2]. However, their limited mechanical properties at elevated temperatures, especially their poor creep resistance, have seriously restricted their industrial use.

In recent years, there has been an increasing interest in the development of high strength and light mass magnesium alloys for application at elevated temperatures. Despite tremendous efforts over the last two decades, currently the Mg-rare earth (RE) alloys are the only magnesium alloy system that can offer adequate creep resistance for applications at temperatures above 200 °C [3]. Among them, the most creep-resistant commercial magnesium alloys developed to date, are those based on alloying with yttrium (Y) and neodymium

(Nd), designated as WE43 (4%Y–3.0%RE–0.5%Zr) and WE54 (5%Y–4%RE–0.5%Zr) by Magnesium Elektron Ltd., U.K. The elevated temperature strength of these alloys is achieved essentially via precipitation hardening. The microstructural evolution and mechanical properties of WE commercial alloys have been well documented [4–6]. They are adequate for long-term service at temperatures up to 250 °C under stressed conditions. A few studies conducted in Japan and China have suggested that the properties of magnesium alloys can be further improved using alloys based on the Mg–Gd and Mg–Dy systems [7–9]. Both Gd and Dy are less common RE elements. Their solubility limits in  $\alpha$ -Mg are 23.5% and 25.8%, respectively. LI et al [10] investigated the microstructure and mechanical properties of as-cast Mg–Gd–Zn alloy, and indicated that this alloy had excellent ultimate tensile strength and yield strength at room temperature. WANG et al [11] reported the effect of Gd addition ranging 2%–4% on the

microstructure and mechanical properties of as-cast Mg–5Y–3Nd–1.0Zr alloy, and found that the mechanical properties were improved at both room temperature and 250 °C. Dy has an identical atomic radius and physical/chemical properties with Gd. Therefore, it is expected that Dy addition would also improve the mechanical properties of Mg–Y–Nd alloys.

The present study is to investigate the effect of a minor addition of Dy on the microstructures and mechanical properties of WE43 alloy, aiming to further improve its performance at elevated temperatures.

## 2 Experimental

The four alloys based on Mg–4Y–3Nd–0.4Zr were investigated. The raw materials were 99.9% Mg, 99.9% Y, 99.5% Dy, Mg–30%Nd master alloy and a Mg–33.3%Zr master alloy. The magnesium alloys were prepared in a boron nitride-coated mild steel crucible in an electrical resistance furnace under a cover gas mixture of 98%CO<sub>2</sub>+2%SF<sub>6</sub> during melting. The magnesium ingot was melted in the steel crucible firstly, and then pure Y and Dy were added at 720 °C. Mg–Nd and Mg–Zr master alloys were added at 750 °C. After stirring, the melt was held at 780 °C for 30 min to ensure the complete dissolution of all alloy elements. RJ5 flux (main compositions: 24%–30% MgCl<sub>2</sub>, 20%–26% KCl, 28%–31% BaCl<sub>2</sub>, 13%–15% CaF<sub>2</sub>, and 8% NaCl+CaCl) was used as a refining agent. Following this procedure, the melts were cast into a sand mould at a pouring temperature of 740 °C.

The nominal chemical compositions were Mg–4%Y–3.2%Nd–0.4%Zr, Mg–4%Y–3.2%Nd–1%Dy–0.4%Zr, Mg–4%Y–3.2%Nd–2%Dy–0.4%Zr, Mg–4%Y–3.2%Nd–3%Dy–0.4%Zr, hereafter denoted as WN, WN-1, WN-2 and WN-3, respectively. The chemical compositions of the alloys measured by inductively coupled plasma atomic emission spectroscopy are given in Table 1.

**Table 1** Chemical compositions of investigated alloys (mass fraction, %)

Alloy	Y	Nd	Dy	Zr	Mg
WN	3.92	3.12	0.0	0.45	Bal.
WN-1	4.06	2.95	0.96	0.42	Bal.
WN-2	3.90	2.92	1.93	0.48	Bal.
WN-3	3.86	3.05	3.04	0.44	Bal.

The castings were solution treated at 525 °C for 8 h, and quenched in 50 °C water, followed by peak aging at 250 °C for 12 h. Metallographic samples were cut from both as-cast and heat-treated castings, and then mounted in cold-setting epoxy resin for microstructural observation. All samples were ground initially with SiC

paper down to a 1200 grit grade, followed by polishing with 6 μm and 1 μm diamond suspensions and finally with colloidal silica suspension. The samples were etched by acetic-picric etchant (5 mL acetic acid, 4.2 g picric acid, 10 mL H<sub>2</sub>O and 50 mL ethanol). The structures of both the as-cast and heat-treated samples were examined using an Olympus BH–2 optical microscope, a FEI Sirion scanning electron microscope (SEM) operating at 20 kV, and a PHILLIPS CM12 transmission electron microscope (TEM) operating at 120 kV. For TEM analysis, disks with 3 mm in diameter were cut from the as-cast and heat-treated castings and ground to a thickness of 70 μm. The thin foils selected for TEM observation were electropolished in a solution (100 mL absolute ethanol, 15 mL 2-butoxyethanol, 3 mL acetic acid, 17.5 g sodium thiocyanate) at –35 to –55 °C with current of 25–30 mA. Before observation, the foils were cleaned by Gatan 691 device using a low energy Ar beam at 253 K. A quantitative energy dispersive spectroscopy (EDS) was then conducted on the thin foil.

Tensile specimens with gauze section of 1.6 mm × 5 mm were cut from the heat-treated castings. The tensile tests at room and elevated temperatures were carried out on a Gleeble–1500D Instron electronic universal materials testing machine with an initial strain rate of 1×10<sup>–3</sup> s<sup>–1</sup> at temperatures up to 300 °C. Prior to testing, the samples were heated at 1 K/s from ambient temperature to the selected temperature, followed by a holding period of 300 s to ensure the uniformity of the temperature. Fractured surface morphologies of failed samples were examined by FEI Sirion SEM.

## 3 Results and discussion

### 3.1 As-cast microstructures

Zirconium is a potential grain refiner for magnesium alloys that contain little (impurity level) or no Al, Mn, Si, Fe, Ni, Co, Sn and Sb because zirconium can form stable and high melting-point compounds with these elements [12]. At a high Zr level of 0.4%, the grain morphology transforms into a distinct rosette-like structure with a dramatic reduction in grain size. There exist Zr particles and Zr-rich cores in the grains, as shown in Fig. 1(a), and the Zr-rich core structure and its line scanning results are given in Figs. 1(b) and (c), respectively. It should be pointed out that many grains contain several particles or Zr-rich cores, as shown in Fig. 1(a) by the arrows.

The SEM images of the WN alloy and its Dy-containing variants are shown in Figs. 2(a)–(d). The average grain size is ~50 μm for all alloys, indicating that the addition of Dy has negligible effect on grain size. When the melt solidifies from a high temperature, α-Mg phase with limited solution of RE forms firstly, then

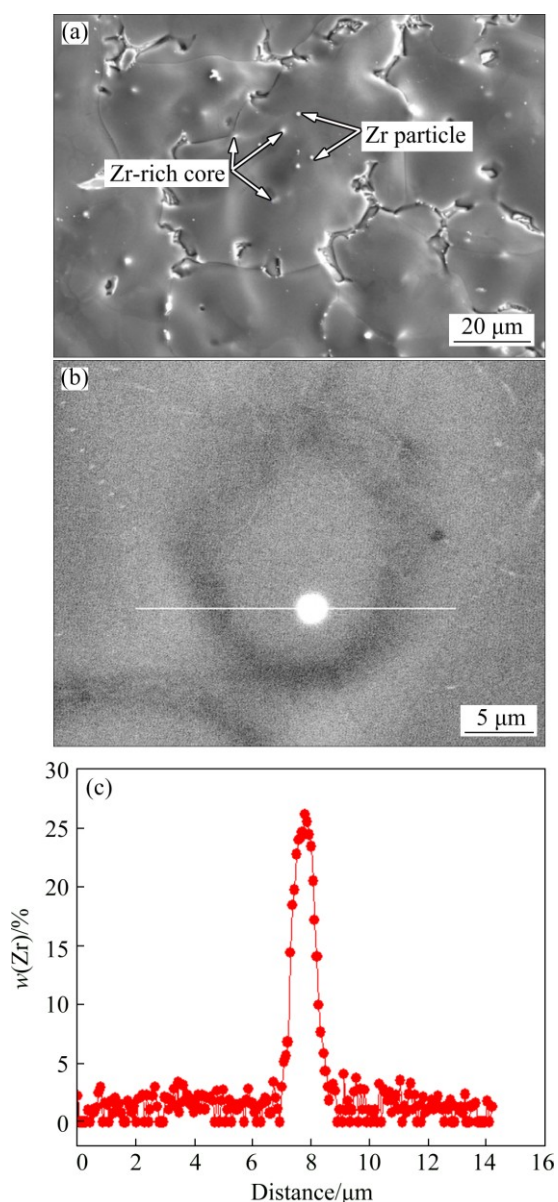


**Fig. 1** SEM image showing Zr particles and Zr-rich cores in WN alloy: (a) WN alloy; (b) Zr-rich core; (c) Zr distribution

other phases such as the eutectic precipitates and intermetallics, form as the temperature decreases.

Owing to the very low solubility of RE in the Mg matrix, the RE elements tend to be concentrated in the eutectic phase along grain boundaries, as shown in Fig. 2. With increasing Dy addition, the amount of Mg–RE eutectic phase increases gradually. Figures 2(e) and (f) are higher magnification images of Figs. 2(a) and (d), respectively. The morphology of eutectic Mg–RE phase is bone-shaped and transfers to a bulky eutectic with increasing Dy element. In addition to the eutectic Mg–RE phase, there are a few fine rectangular-shaped Mg–RE phase particles that display a brighter contrast than the eutectic Mg–RE phase, occurring in close association with the eutectic phase, as indicated by the

arrows in Figs. 2(e) and (f). The Mg–RE with a bright contrast phase within the eutectic phase implies that these Mg–RE particles may act as the nucleation sites of the eutectic phase during solidification [13].

TEM images of the WN alloy are shown in Fig. 3. An image of the eutectic compound together with some fine rectangular intermetallic particles is shown in Fig. 3(a), and their corresponding selected area electron diffraction (SAED) patterns are given in Figs. 3(b) and (c), respectively. The SAED patterns indicate a face-centered cubic crystal (FCC) structure with  $a=2.244$  nm for the eutectic compound, and the fine rectangular phase near the divorced eutectic compound also has an FCC structure ( $a=0.519$  nm).

The EDS analyses in TEM are shown in Fig. 4. The typical average chemical composition of the bone-shaped eutectic compound is approximately 82.38%Mg–4.83%Y–12.79%Nd, as shown in Fig. 4(a), indicating that the eutectic phase is the  $Mg_5RE$  phase, in which the RE is a mixture of Nd and Y elements. The mole ratio of Nd:Y in the bone-shaped eutectic precipitates is  $\sim 2.65:1$ . Comparing with the results of the eutectic phase observed in the Mg–Y–Nd alloy by APPS et al [14], the eutectic phase is suggested to be stoichiometry of  $Mg_5(Y_{0.28}Nd_{0.72})$ . Near the large divorced eutectic compound, there are a few fine rectangular particles with a size of  $\sim 0.2$  μm, as shown by arrows in Fig. 2(e). The relatively small size of the rectangular intermetallic compound is likely to contain significant information from the surrounding matrix, resulting in more diluted compound for analysis than the true composition. Their compositions are determined to be approximately 16.48%Mg–71.08%Y–12.44%Nd from the EDS spectrum analysis using the extrapolation technique described by LORIMER et al [15], as shown in Fig. 4(b). This implies that its stoichiometry is near  $Mg_3RE_{17}$ , where RE represents a mixture of RE elements in the mole ratio of Y:Nd=5.5:1, suggesting a stoichiometry of  $Mg_3(Y_{14.4}Nd_{2.6})$ .

A TEM image of eutectic compound and fine rectangular intermetallic particles is shown in Fig. 5(a), and their corresponding SAED patterns are given in Figs. 5(b) and (c) for the WN-2 alloy. The SAED patterns indicate an FCC crystal structure with a lattice parameter of  $a=2.244$  nm for the eutectic compound, and the structure of the fine rectangular phase near the eutectic compound is also an FCC crystal structure with a lattice parameter of  $a=0.519$  nm.

The EDS analyses for the as-cast WN-2 alloy in TEM are shown in Fig. 6. The typical average content of the bone-shaped eutectic compound is approximately 84.82%Mg–4.67%Y–9.7%Nd–0.81%Dy as shown in Fig. 6(a) which corresponds to  $Mg_5RE$ , where RE is a

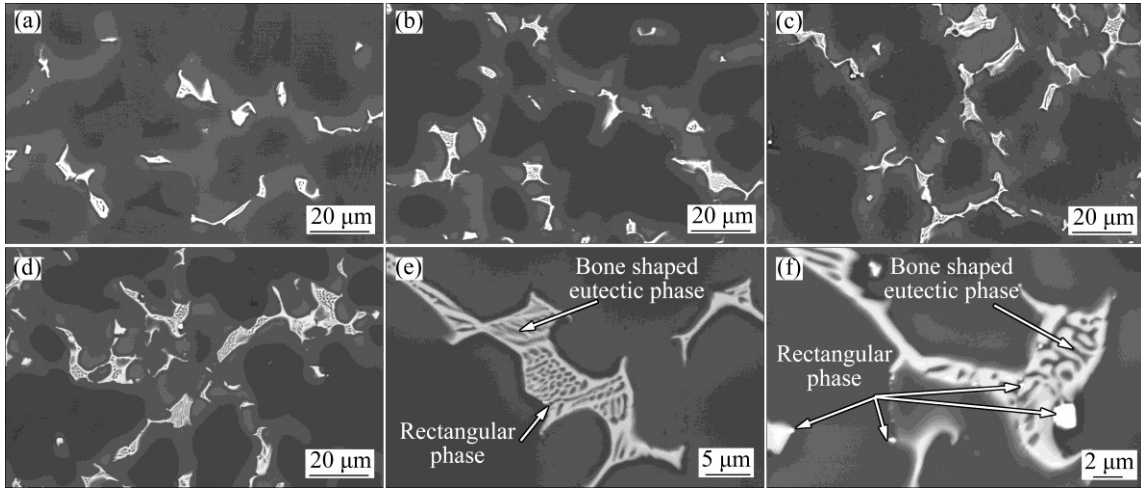


**Fig. 2** SEM images of as-cast WN alloys: (a) WN; (b) WN-1; (c) WN-2; (d) WN-3; (e) Enlarged image of (a); (f) Enlarged image of (d)

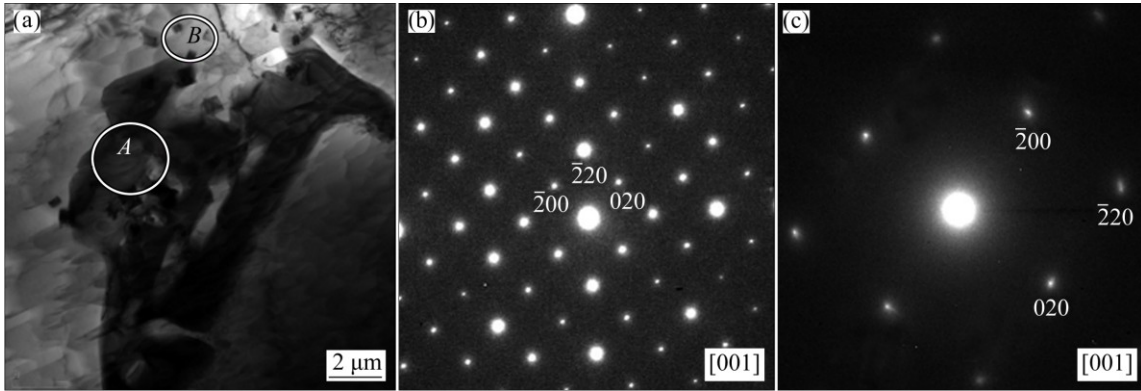


**Fig. 3** TEM BF image and corresponding SAED patterns of WN alloy: (a) TEM image of WN; (b) SAED pattern of eutectic phase in A; (c) SAED pattern of rectangular phase in B

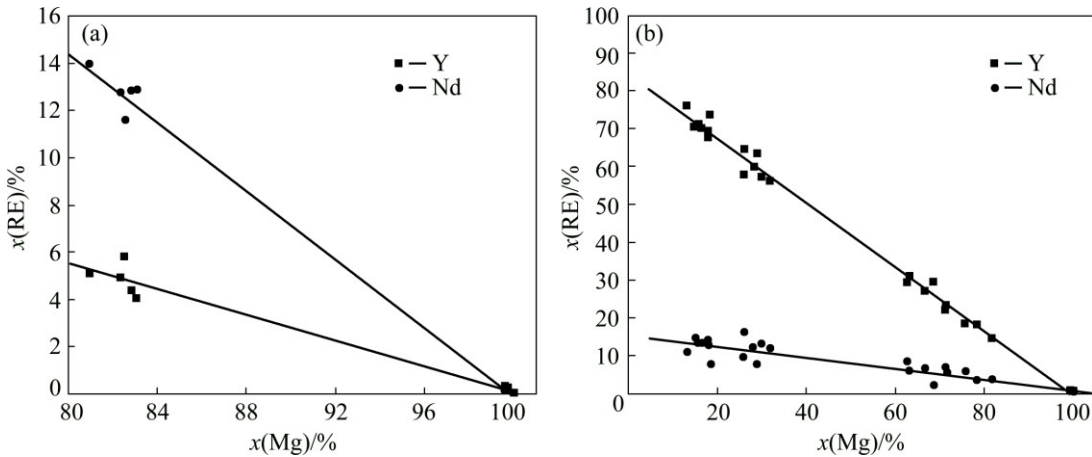


**Fig. 4** Concentration of Y and Nd in different phases of WN alloy: (a) In eutectic phase; (b) In rectangle phase (Bone-shaped eutectic phase is  $Mg_5(Y_{0.28}Nd_{0.72})$  and rectangular phase is  $Mg_3(Y_{14.4}Nd_{2.6})$ )

mixture of Y, Nd and Dy. The mole ratio of the RE elements in the bone-shaped eutectic precipitate is  $\sim Y:Nd:Dy=6:13:1$ , suggesting a stoichiometry of  $Mg_5(Y_{0.3}Nd_{0.65}Dy_{0.05})$ . The fine rectangular phase possesses approximately 14.8% Mg–59.8%Y–11.24%Nd–14.16%Dy, as shown in Fig. 6(b) determined

by the extrapolation technique, indicating that its stoichiometry is near  $Mg_3RE_{17}$ , where RE is a mixture of RE elements of Y, Nd and Dy. The mole ratio of the RE elements present in the rectangular precipitate is  $\sim Y:Nd:Dy=12.0:2.2:2.8$ , suggesting a stoichiometry of  $Mg_3(Y_{12}Nd_{2.2}Dy_{2.8})$ .

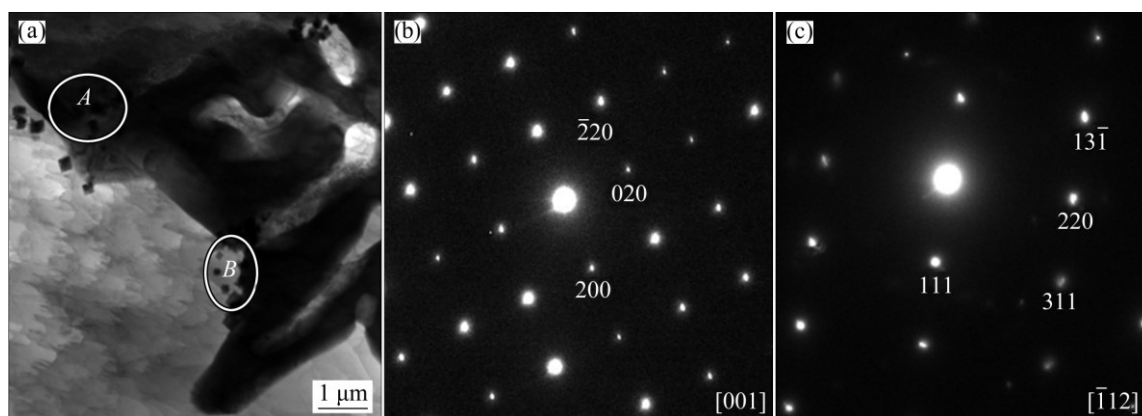


**Fig. 5** TEM BF image and corresponding SAED patterns of WN-2 alloy: (a) TEM of WN-2; (b) SAED pattern of eutectic phase in *A*; (c) SAED pattern of fine rectangular phase in *B*

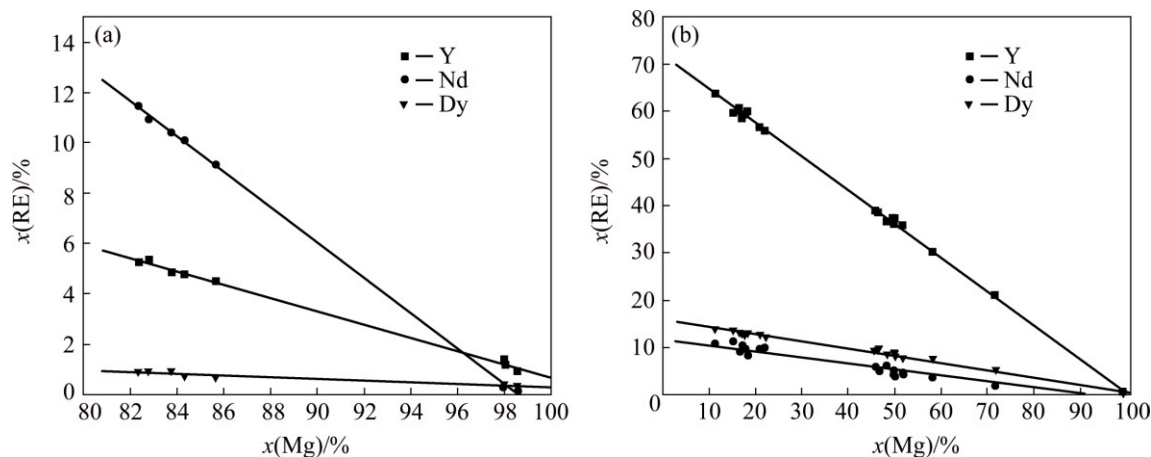


**Fig. 6** Content of Y, Nd and Dy in different phases of WN-2 alloy: (a) In eutectic phase; (b) In rectangle phase (eutectic phase is likely  $\text{Mg}_5(\text{Y}_{0.3}\text{Nd}_{0.65}\text{Dy}_{0.05})$  and rectangular phase is  $\text{Mg}_3(\text{Y}_{12}\text{Nd}_{2.2}\text{Dy}_{2.8})$ )

The eutectic  $\text{Mg}_5\text{RE}$  is rich in Nd element and the rectangular phase is rich in Y element. There is no change in phase structure and lattice parameters for the WN alloy by addition of Dy except the increased volume fraction of Mg–RE phase.

### 3.2 Microstructures of heat-treated Mg alloy

The alloys were solution treated at 525 °C for 8 h. After solution treatment, the  $\text{Mg}_5\text{RE}$  eutectic phase, distributed along the grain boundaries in the as-cast samples, is dissolved completely into the matrix. The 8 h solid solution treatment at 525 °C enables the significant grain hexagonalization. The average grain size after heat treatment is  $(60 \pm 6)$  μm, slightly higher than that of the as-cast alloy due to some fine grains amalgamating. However, the composition, morphology and structure of the rectangular  $\text{Mg}_3\text{RE}_{17}$  phase remained unchanged, suggesting its higher thermal stability, as shown by the arrows in Fig. 7. After aging, the Mg–RE phases precipitate uniformly. TEM images for peak-aged samples are shown in Fig. 8, indicating that the addition of Dy can favor the formation of finer and uniform

precipitated Mg–RE phases.

### 3.3 Effect of Dy on mechanical properties at elevated temperature

The mechanical properties at elevated temperatures up to 300 °C are summarized in Table 2. The tensile strengths of Dy-containing WN variants increase gradually with the increasing Dy addition. 3% Dy addition results in increase in tensile strength of the WN-3 alloy by 17.5%, 38% and 45% at room temperature, 250 °C and 300 °C, respectively. Even at 300 °C, the tensile strength can reach up to 252 MPa, whereas, the elongation to failure decreases.

The elevated temperature strength of WE alloys is achieved essentially via precipitation hardening. The precipitated sequence in Mg–Y–Nd alloys is the formation of  $\beta'$ ,  $\beta''$  and  $\beta$  phase particles, depending upon aging temperature [6,7]. The metastable phase  $\beta'$  has a D019 crystal structure (hexagonal,  $a=0.642$  nm,  $c=0.521$  nm). The intermediate phase  $\beta''$  has a base-centered orthorhombic structure ( $a=0.640$  nm,  $b=2.223$  nm,  $c=0.521$  nm), and the equilibrium phase  $\beta$

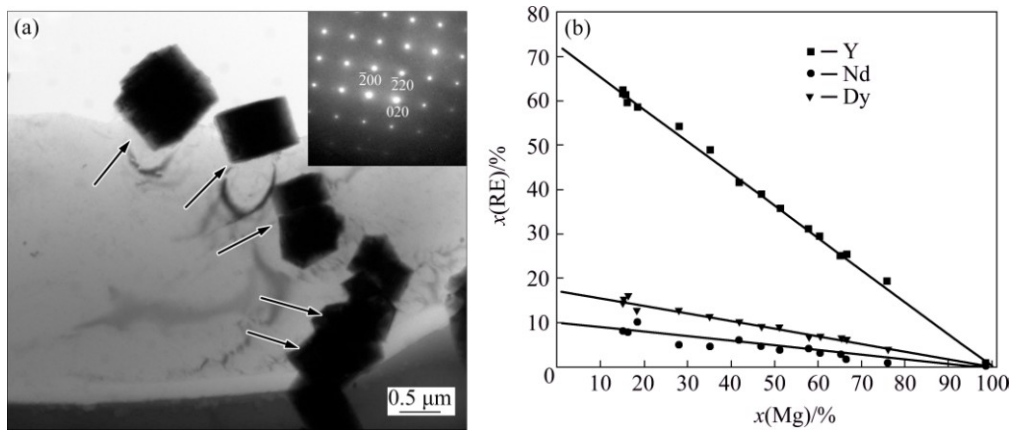


**Fig. 7** TEM image of solution-treated WN-2 alloy (a) and contents of Y, Nd and Dy in rectangular phase (b) (Rectangular phase is  $\text{Mg}_3(\text{Y}_{12.4}\text{Nd}_{3.0}\text{Dy}_{1.6})$ )

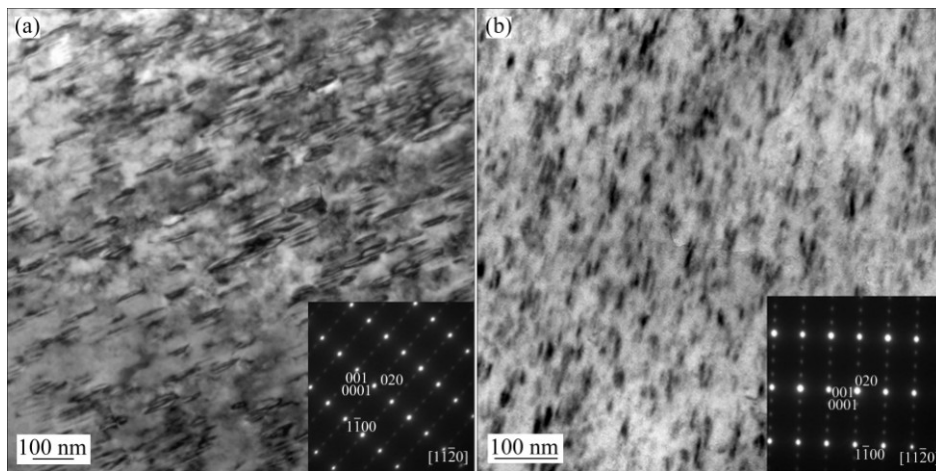


**Fig. 8** Bright-field TEM images of peak-aged alloys: (a) WN; (b) WN-2

**Table 2** Tensile mechanical properties at both room and elevated temperature for WN alloys

Alloy	RT			250 °C			300 °C		
	$\sigma_{0.2}$ /MPa	$\sigma_b$ /MPa	$\delta$ /%	$\sigma_{0.2}$ /MPa	$\sigma_b$ /MPa	$\delta$ /%	$\sigma_{0.2}$ /MPa	$\sigma_b$ /MPa	$\delta$ /%
WN	175	272	6.5	146	216	12.8	135	173	24
WN1	204	302	5.8	178	273	10.4	159	224	19.8
WN2	210	307	5.0	193	292	9.8	176	238	12.6
WN3	215	315	4.5	202	305	8.8	185	252	10.8

is face-centered cubic ( $a=2.223$  nm). Under peak aging at 250 °C, the precipitate mainly consists of  $\beta'$  phase [6]. The effects of alloying elements on the mechanical properties of the alloys have been found to be related to the volume fraction and type of intermetallic phases [16]. There is no change in the type of precipitate after Dy addition to the WE43 alloy, but the total mass fraction of Mg–RE precipitated phases in the Dy-containing alloys is higher than that in the WN alloy due to the higher content of RE elements, as shown in Fig. 8. On one hand, the solubility of RE is decreased by multi-rare earth element additions, resulting in an enhanced amount of precipitates even with the same addition amount. The

strength of alloy is increased by inhibiting the movement of grain boundaries and pinning up dislocations at the elevated temperature. On the other hand, an increased amount of second phase is expected to generally decrease the elongation to fracture by providing nucleation sites for voids and micro-cracks. This is the reason why 3% Dy addition results in a slight decrease in elongation.

#### 4 Conclusions

1) The as-cast microstructures of the WN alloy and its Dy-containing variants consist of primary  $\alpha$ -Mg phase,

bone-shaped eutectic  $Mg_5RE$  and rectangular  $Mg_3RE_{17}$  phases. The amount of precipitated  $Mg-RE$  compounds increases with Dy addition without the formation of new phases. After solution treatment, the eutectic  $Mg_5RE$  is completely dissolved into the matrix, while rectangular  $Mg_3RE_{17}$  compounds remains, indicating that the  $Mg_3RE_{17}$  has excellent thermal stability.

2) Dy addition improves the mechanical properties of WN alloy significantly at both room and elevated temperatures, especially at the elevated temperature. At 300 °C, an increase of 45% in tensile strength is obtained after 3% Dy addition, which is attributed to the enhanced amount of precipitates.

## References

- [1] YANG Ming-bo, WU De-yong, HOU Meng-dan, PAN Fu-sheng. As-cast microstructures and mechanical properties of  $Mg-4Zn-xY-1Ca$  ( $x=1.0, 1.5, 2.0, 3.0$ ) magnesium alloys [J]. Transactions of Nonferrous Metals Society of China, 2015, 25(3): 721–732.
- [2] MEI Jun, LIU Wen-cai, WU Guo-hua, ZHANG Yang, ZHANG Yi-tao, HONG Yi-kai, ZHANG Ruo-xi, XIAO Lu, DING Wen-jiang. Effect of complex melt-refining treatment on microstructure and mechanical properties of sand-cast  $Mg-10Gd-3Y-0.5Zr$  alloy [J]. Transactions of Nonferrous Metals Society of China, 2015, 25(6): 1811–1821.
- [3] NING Zhi-liang, YI Jun-ying, QIAN Ma, SUN Hai-chao, CAO Fu-yang, LIU Hong-hui, SUN Jian-fei. Microstructure and elevated temperature mechanical and creep properties of  $Mg-4Y-3Nd-0.5Zr$  alloy in the production form of a large structural casting [J]. Materials and Design, 2014, 60(8): 218–225.
- [4] KUMAR N, DENDGE N, BANERJEE R, MISHRA R S. Effect of microstructure on the uniaxial tensile deformation behavior of  $Mg-4Y-3RE$  alloy [J]. Materials Science and Engineering A, 2014, 590(1): 116–131.
- [5] KANDALAM S, AGRAWAL P, AVADHANI G S, KUMAR S, SUWAS S. Precipitation response of the magnesium alloy WE43 in strained and unstrained conditions [J]. Journal of Alloys and Compounds, 2014, 623: 317–323.
- [6] BARUCCA G, FERRAGUT R, FIORI F, LUSSANA D, MENGUCCI P, MOIA F, RIONTINO G. Formation and evolution of the hardening precipitates in a  $Mg-Y-Nd$  alloy [J]. Acta Materialia, 2011, 59(10): 4151–4158.
- [7] CAO Liang, LIU Wen-cai, LI Zhong-quan, WU Guo-hua, XIAO Lu, WANG Shao-hua, DING Wen-jiang. Effect of heat treatment on microstructures and mechanical properties of sand-cast  $Mg-10Gd-3Y-0.5Zr$  magnesium alloy [J]. Transactions of Nonferrous Metals Society of China, 2014, 24(3): 611–618.
- [8] LI Y X, ZHU G Z, QIU D, YIN D D, RONG Y H, ZHANG M X. The intrinsic effect of long period stacking ordered phases on mechanical properties in  $Mg-RE$  based alloys [J]. Journal of Alloys and Compounds, 2016, 660: 252–257.
- [9] JUNG I H, SANJARI M, KIM J, YUE S. Role of RE in the deformation and recrystallization of Mg alloy and a new design concept for  $Mg-RE$  alloys [J]. Scripta Materialia, 2015, 102: 1–6.
- [10] LI J C, HE Z L, FU P H, WU Y J, PENG L M, DING W J. Heat treatment and mechanical properties of a high-strength cast  $Mg-Gd-Zn$  alloy [J]. Materials Science and Engineering A, 2016, 651: 745–752.
- [11] WANG L, XING C, HOU X, WU Y, SUN J, WANG L. Microstructures and mechanical properties of as-cast  $Mg-5Y-3Nd-Zr-xGd$  ( $x=0, 2$  and 4wt.%) alloys [J]. Materials Science and Engineering A, 2010, 527(7): 1891–1895.
- [12] QIAN M, HILDEBRAND Z C G, STJOHN D H. The loss of dissolved zirconium in zirconium-refined magnesium alloy after remelting [J]. Metallurgical and Materials Transaction A, 2009, 40(10): 2470–2479.
- [13] GOLMAKANIYOON S, MAHMUDI R. Comparison of the effects of La- and Ce-rich rare earth additions on the microstructure, creep resistance, and high-temperature mechanical properties of  $Mg-6Zn-3Cu$  cast alloy [J]. Materials Science and Engineering A, 2011, 528(15): 5228–5233.
- [14] APPS P J, KARIMZADEH H, KING J F, LORIMER G W. Phase compositions in magnesium-rare earth alloys containing yttrium, gadolinium or dysprosium [J]. Scripta Materialia, 2003, 48(5): 475–481.
- [15] LORIMER G, CLIFF G, CHAMPNESS P, DICKINSON C, HASAN F, KENWAY P. Analytical electron microscopy [M]. San Francisco: San Francisco Press, 1994.
- [16] CHIA T L, EASTON M A, ZHU S M, GIBSON M A, BIRBILIS N, NIE J F. The effect of alloy composition on the microstructure and tensile properties of binary  $Mg$ -rare earth alloys [J]. Intermetallics, 2009, 17(7): 481–490.

## 镧添加对 $Mg-4Y-3Nd-0.4Zr$ 合金组织和力学性能的影响

刘洪汇<sup>1,2</sup>, 宁志良<sup>1,2</sup>, 伊军英<sup>1,3</sup>, Qian MA<sup>4</sup>, 孙海超<sup>1,2</sup>, 黄永江<sup>1,2</sup>, 孙剑飞<sup>1,2</sup>

1. 哈尔滨工业大学 材料科学与工程学院, 哈尔滨 150001;

2. 哈尔滨工业大学 金属精密热加工国家级重点实验室, 哈尔滨 150001;

3. 江苏科技大学 材料科学与工程学院, 张家港 215600;

4. Mechanical and Manufacturing Engineering and Design Research Institute,

School of Aerospace, RMIT University, GPO Box 2476, Melbourne, VIC 3001, Australia

**摘要:** 研究了镧元素添加对  $Mg-4Y-3Nd-0.4Zr$  合金显微组织和力学性能的影响, 并采用扫描电镜和透射电镜观察合金的显微组织。结果表明, 铸态合金中的共晶相和方形块状  $Mg-RE$  相分别为  $Mg_5RE$  相和  $Mg_3RE_{17}$  相, 主要分布在晶界位置。经固溶处理后,  $Mg_5RE$  共晶相溶入基体中, 而  $Mg_3RE_{17}$  金属间化合物依然存在。时效后, 添加镧元素的合金  $Mg-RE$  析出相分布更均匀, 显著提高了合金的室温和高温抗拉强度, 但伸长率略有下降。

**关键词:** 镁合金; 镧元素添加; 显微组织; 力学性能

(Edited by Xiang-qun LI)